ICAS 2016
30th Congress of the International Council of the Aeronautical Sciences
DCC, Daejeon, Korea ; September 25-30, 2016

EXTENDED LOCAL SCATTERING THEORY AND THE ROLE OF A SCATTER ON BOUNDARY-LAYER INSTABILITY AND ACOUSTIC RADIATION

Ming Dong*,, Xuesong Wu*,****
*** Department of Mathematics, Imperial College London, SW7 2AZ, UK**
**** Department of Mechanics, Tianjin University, Tianjin, 300072, China**

Keywords: *boundary layer, scattering, instability, acoustic radiation,*

Abstract

In this paper, we propose a theoretical framework, referred to as the Extended Local Scattering Theory, to study the sound generation due to scattering of an oncoming Tollmien-Schliching (T-S) wave by a local scatter in subsonic boundary layers. In this framework, a transmission coefficient, defined as the ratio of the T-S wave amplitude downstream of the scatter to that upstream, is introduced to characterize the effect of a local scatter on boundary-layer instability. The mathematical formulation is based on the triple-deck formalism, but in order to accommodate the acoustic far field, the unsteady (second-order) terms in the upper-deck equations, which play a leading-order role in acoustic radiation, are retained. This approach also includes the influence of the radiated sound wave on the near-wall hydrodynamic perturbation. Through computation, the impacts of a steady local suction on the hydrodynamic instability and acoustic radiation are studied.

1 Introduction

When a boundary-layer instability mode propagates through a region of streamwise rapid distortion, the ensuing scattering causes two consequences of physical interest. First, the amplitude of the instability mode may be suppressed or energized, through which the instability and transition is influenced. Second, if the flow is compressible, a sound wave of substantial intensity can be radiated to the far field.

This paper focuses on this issue by extending the recently developed Local Scattering framework. The central idea of this framework is to treat the abrupt change as a scatter, and wave activities in its vicinity as a scattering problem, while in the relatively smooth regions away from the abrupt change, the disturbance evolves as an instability mode. Since the mean flow in the smooth regions varies slowly along the streamwise direction, the evolution of the disturbances can be described by the classical linear stability theory or parabolised stability equations (PSE). These approaches however cease to be valid when the perturbations propagate through a rapidly distorting mean flow that occurs over a length scale comparable with the characteristic wavelength of the instability modes.

The earliest idea of introducing the transmission coefficient to characterize the impact of a hump on hydrodynamic instability was proposed by Wu & Hogg [1]. In that work, the governing equations were based on triple-deck formalism [2, 3], and the analytical solution was obtained by assuming the hump to be sufficiently small. However, the small hump was found to exert a rather weak impact on the oncoming T-S wave because the linear limit turned out to be a degenerated problem with the transmission coefficient being unity to leading-order approximation, and only by proceeding to the second order in the analysis is a non-unity transmission obtained.

In order to solve the problems for large-roughness cases, Wu & Dong [4] recently proposed the first version of the Local

Scattering Theory, in which a complete theory and numerical approach to describe the impact of a scatter on hydrodynamic instability were proposed. Since the eigenfunctions of the T-S wave at the sufficiently upstream and downstream locations are of the same shape, the perturbations at these two locations are related by the transmission coefficient, leading to a quiasi-periodic like boundary condition in the streamwise direction. A numerical approach for solving the boundary-value problem was developed.

In the compressible case, a sound wave is radiated. In order to accommodate sound radiation in the far field, an outer acoustic region needs to be introduced, where the unsteady perturbation is governed by the convected wave equation [1]. However, as suggested by Wu [5], a formal introduction of the acoustic region can be avoided by retaining in the upper-deck equations the second-order (unsteady) terms, which play a leading-order role in radiation in the acoustic region. Therefore, in this paper, we will extend the Local Scattering Theory by this means. The physical model to be studied is a boundary-layer flow with a local steady suction, which is regarded as an efficient strategy for laminar flow control in many applications.

2 Formulations

2.1 Physical model

As shown in Fig. 1, the physical model to be studied is a two-dimensional compressible boundary layer over a semi-infinite flat plate, with a localized steady suction through a slot whose centre is at a distance L downstream of the leading edge. Let $U_\infty, a_\infty, \rho_\infty, T_\infty$ and μ_∞ denote the free-stream velocity, sound speed, density, temperature and dynamical viscosity. We define the Mach number and Reynolds number as

$$M = U_\infty / a_\infty, \quad R = \rho_\infty U_\infty L / \mu_\infty .$$

In this paper, we take $M < 1$ and $R >> 1$. The flow is described in the Cartesian coordinate system (x^*, y^*) with its origin at the centre of the suction slot.

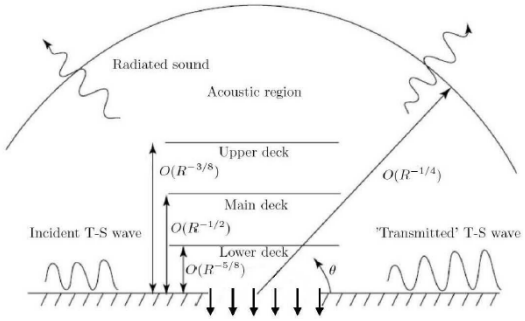

Figure 1 Sketch of the physical model

2.2 Triple-deck scalings

According to the triple-deck formalism, we introduce a small parameter

$$\varepsilon = R^{-1/8},$$

and then there appear three decks in the wall-normal direction. The widths of which are scaling of $O(\varepsilon^5), O(\varepsilon^4)$ and $O(\varepsilon^3)$; these are referred to as the lower-, main- and upper-decks, respectively. The detailed expression can be seen in Dong and Wu [6]. Let $(Y, u, v), (\tilde{y}, \tilde{u}, \tilde{v})$ and $(\bar{y}, \bar{u}, \bar{v})$ denote the normalized wall-normal coordinate, streamwise and wall-normal velocities at lower-, main- and upper- decks, respectively, while $(X, T, p, \alpha, \omega)$ denote the normalized streamwise coordinate, time, pressure, streamwise wavenumber and frequency for all decks, respectively.

2.3 Mean flow and the unsteady perturbation

The flow field associating with the interaction between an oncoming T-S wave and a local steady suction is decomposed as

$$(u, v, p) = (U, V, P) + \bar{\varepsilon}(\tilde{u}, \tilde{v}, \tilde{p})e^{-i\omega T} + c.c., \quad (1)$$

where the first and second terms of the right-hand side denotes the mean flow and the perturbation, respectively, and the amplitude of the perturbation $\bar{\varepsilon}$ is assumed to be sufficiently small.

The suction slot is assumed to have a width of $O(R^{-3/8}L)$, and the suction velocity is of $O(R^{-3/8}U_\infty)$ or smaller. The boundary condition on the local mean-flow distortion is

$$V(X, 0) = V_s(X).$$

The governing equations and the numerical

approaches for the mean flow can be found in Wu & Dong [4], and the only difference is the boundary condition of the wall-normal velocity at the wall. The governing equations of the unsteady perturbations are the boundary-layer equations

$$\begin{aligned} &\tilde{u}_X + \tilde{v}_Y = 0, \\ &(-i\omega + U_X)\tilde{u} + U_Y\tilde{v} + U\tilde{u}_X + V\tilde{u}_Y + \tilde{p}_X - \tilde{u}_{YY} = 0, \end{aligned} \tag{2}$$

subject to the boundary conditions at the wall and matching condition with with the main-deck solution,

$$\begin{aligned} &\tilde{u} = \tilde{v} = 0 \qquad at\ Y = 0, \\ &\tilde{u} \to \tilde{A}(X) \qquad as\ Y \to \infty, \end{aligned} \tag{3}$$

where the displacement function $\tilde{A}(X)$ and the pressure $\tilde{p}(X)$ of the unsteady perturbation satisfy the pressure-displacement relation (P-D law), which is to be derived by matching with the upper-deck equations.

Let the pressure in the upper deck be written as $\bar{p}(X,\bar{y})e^{-i\omega T}$, and further introduce

$$\bar{p}^+ = e^{i\hat{s}MX}\bar{p}, \quad \hat{s} = \varepsilon_0\omega M/(1-M^2), \tag{4}$$

Where $\varepsilon_0 = \lambda^{1/4}(1-M^2)^{-1/8}C^{1/8}T_w^{1/2}\varepsilon$, with λ, C, T_w being the wall shear of the Blasius profile, the constant of the Chapman viscosity law and the wall temperature.

It follows that $\bar{p}^+$ satisfies

$$\begin{aligned} &\bar{p}^+_{XX} + \bar{p}^+_{\bar{y}\bar{y}} + \hat{s}\bar{p}^+ = 0, \\ &P^+_{\bar{y}}(X,0) = e^{i\hat{s}MX}(\frac{\partial}{\partial X} - i\varepsilon_0\omega)^2\tilde{A}(X). \end{aligned} \tag{5}$$

Taking the Fourier transform with respect to X, we can solve the above system to obtain

$$\hat{p}^+ = -\frac{1}{\kappa}e^{-\kappa\bar{y}}[i(k-M\hat{s}) - i\varepsilon_0\omega]^2\hat{A}(k-M\hat{s}), \tag{6}$$

where $\hat{p}^+$ and $\hat{A}$ denote the Fourier transform of $\bar{p}^+$ and $\tilde{A}$, respectively, and

$$\kappa \equiv \begin{cases} -i(\hat{s}^2-k^2)^{1/2} & for\,|k| < \hat{s}, \\ (k^2-\hat{s}^2)^{1/2} & for\,|k| \geq \hat{s}. \end{cases}$$

For $\bar{y} = 0$, we may invert (6) by using the convolution theorem to obtain $\bar{p}^+$, which is then inserted into (4) to give the pressure at $\bar{y} = 0$,

$$\tilde{p}(X) = \int_{-\infty}^{\infty} G(X-\xi)e^{-iM\hat{s}(X-\xi)}(\frac{\partial}{\partial\xi} - i\varepsilon_0\omega)^2\tilde{A}(\xi)d\xi, \tag{7}$$

where the Green's function is expressed as

$$G(\zeta) = \frac{1}{\pi}\{-\int_{\hat{s}}^{\infty}\frac{\cos(k\zeta)}{\sqrt{k^2-\hat{s}^2}}dk - i\int_0^{\hat{s}}\frac{\cos(k\zeta)}{\sqrt{\hat{s}^2-k^2}}dk\}$$

for $\zeta \neq 0$.

Equation (7) is the generalized P-D law, which accounts for acoustic radiation.

The transmission coefficient T is defined as the ratio of the amplitude of the T-S wave downstream of the suction slot to that upstream. With the aid of T, the asymptotic behaviors of the unsteady perturbation in the upstream and downstream limits are expressed as

$$(\tilde{u},\tilde{v},\tilde{p}) \to (\hat{u},\hat{v},\hat{p})e^{i\alpha X} + \bar{P}(X)(\hat{u}_S,\hat{v}_S,\hat{p}_S) \quad as\ X \to -\infty, \tag{8}$$

$$(\tilde{u},\tilde{v},\tilde{p}) \to T(\hat{u},\hat{v},\hat{p})e^{i\alpha X}(1+O(X^{-\tau})) \quad as\ X \to -\infty, \tag{9}$$

where $(\hat{u},\hat{v},\hat{p})$ is the eigenfunction of the oncoming T-S wave with α being its wavenumber, while $(\hat{u}_S,\hat{v}_S,\hat{p}_S)$ stands for the Stokes-shear wave generated by the radiated sound wave in the free stream, with its amplitude being $\bar{P}(X)$. The terms of $O(X^{-\tau})$ in (9) is due to the transmitted T-S wave being re-scattered by the wake of the scatter, which is neglected in this paper because the mean flow is truncated at a downstream location.

2.4 Discretization

Let the computational domain in the lower deck $X_0 \le X \le X_I$ and $Y_0 \le Y \le Y_J$ be divided into rectangular cells by a grid consisting of $I+1$ lines in X direction with the width $\Delta_X = X_i - X_{i-1}$, and a non-uniform mesh is used in the Y direction with the width at each interval $\Delta_{Y_j} = Y_j - Y_{j-1}$. The mean flow can be calculated by the same method as that introduced in Wu & Dong [4].

The system governing the unsteady perturbation consists of the lower-deck equations (2), the boundary conditions (3), the P-D law (7) and the upstream- and the downstream- asymptotic conditions (8) and (9). The system can be discretized by similar

approaches as those in Wu & Dong [4]. For a finite computational domain, the perturbation field for the inlet boundary condition (8) and outlet boundary condition (9) can be recast to a 'quasi-periodic' type of condition,

$$\tilde{\phi}_I = Te^{i\alpha(X_I - X_0)}(\tilde{\phi}_0 - \bar{P}_0\tilde{\phi}_S), \quad (10)$$

where $\tilde{\phi}$ denotes (u, v, p), $\tilde{\phi}_S$ represents the Stokes layer, and $\bar{P}_0 = \bar{P}(X_0)$, and $\tilde{\phi}_I$ represents the perturbation to be solved

2.5 Eigenvalue framework for the local scattering problem

Let the unknown variables be written as a vector

$$\boldsymbol{\varphi} = [\varphi_{00}, \varphi_{01}, \cdots, \varphi_{IJ}, \tilde{p}_0, \tilde{p}_1, \cdots, \tilde{p}_I, \bar{P}_0]^T. \quad (11)$$

where $\varphi_{ij} = (\tilde{u}_{ij}, \tilde{v}_{ij}, \tilde{u}_{Y,ij})$. The discrete system can be written as a linear eigenvalue problem of the form

$$\mathbf{A}\boldsymbol{\varphi} = \mathcal{T}\mathbf{B}\boldsymbol{\varphi}, \quad (12)$$

where $\mathbf{A}$ and $\mathbf{B}$ are coefficient matrices, whose expression can be obtained by similar method of Wu & Dong [4], and $\mathcal{T}$ is the eigenvalue of the system.

2.6 Far-field sound

The pressure in the acoustic zone is given by

$$p_s = \frac{1}{2\pi}\int_{-\infty}^{\infty} \frac{e^{i(k-M\hat{s})X - \kappa y}}{\kappa}(k - Ms - \varepsilon_0\omega)^2 \hat{A}(k - M\hat{s})dk \quad (13)$$

Use of stationary-phase method shows that in the far field

$$\bar{r} = (X^2 + \bar{y}^2)^{1/2} >> O(\varepsilon^{-1}),$$

the pressure is expressed as

$$p_s = \frac{i\hat{s}^2 M^{-2}(1 - M\cos\theta)^2}{(2\pi\bar{r}\hat{s})^{1/2}}\hat{A}(k_s)e^{i[\hat{s}(\bar{r} - MX) - \frac{\pi}{4}]}, \quad (14)$$

where $\theta = \tan^{-1}(\bar{y}/X)$, and $k_s = \hat{s}(-M + \cos\theta)$.

Since the Stokes layer in (8) is generated by the upstream propagating acoustic wave, as $X \to -\infty$, we have

$$\bar{P}(X) \to p_s(\theta = \pi),$$

and so

$$\bar{P}(X_i) \to \bar{P}_0\left(\frac{X_i}{X_0}\right)^{-1/2} e^{-i\hat{s}(1+M)(X_i - X_0)}. \quad (15)$$

3 Numerical results

3.1 Steady mean flow

We consider the case of the suction velocity distribution being Gaussian, i.e.

$$V_s(X) = V_{s0}\exp(-X^2/d^2), \quad (16)$$

where V_{s0} is the suction velocity at the slot centre, which is negative/positive for a suction/injection, and d characterizes the width of the suction slot.

Fig. 2-(a) displays the streamwise distribution of the normalized pressure $P(X)/|V_{s0}|$ for different suction/injection velocities. In general, suction produces a sharp adverse pressure gradient in the vicinity of the slot centre $X = 0$, and gradual favorable pressure gradients in the regions upstream and downstream. The opposite is true for injection. The pressure tends to be zero as $X \to \pm\infty$. The displacement function, as shown in Fig. 2-(b), also undergoes a sharp increase/decrease in the vicinity of the slot centre for the suction/injection case. However, after $X \approx 2$, it approaches zero at a much slower rate as $X \to \infty$ than the pressure does. For $|V_{s0}| \le 0.1$, the mean-flow distortion increases with the $|V_{s0}|$ proportionally, and has opposite signs for $\pm V_{s0}$. However, obvious differences on $P(X)/|V_{s0}|$ and $A(X)/|V_{s0}|$ are observed for $|V_{s0}| = 1.0$ from those for $|V_{s0}| \le 0.1$ due to the nonlinear effect coming into play at large suction or injection velocities.

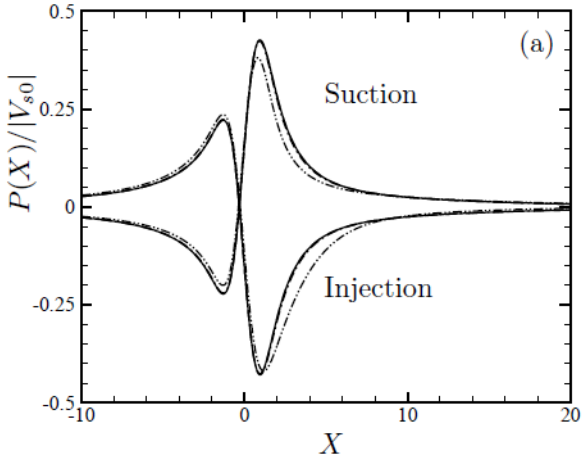

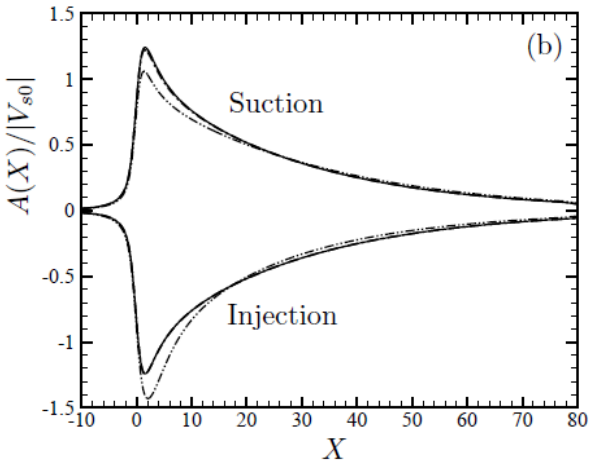

Figure 2 The normalized pressure (a) and displacement function (b) for a suction/injection slot with $d = 1.0$ and different suction/injection velocities. Solid, dashed, dot-dashed and dot-dot-dashed lines represent $|V_{s0}| = 0.001$, 0.01, 0.1 and 1.0, respectively.

3.2 Scattering effect on T-S wave

Including the second-order terms in the upper-deck governing equations leads to a modification of the dispersion relation of the T-S wave, as was shown in Fig. 2 and 3 of Dong & Wu [6]. For $M = 0.2$ and $R = 10^6$, the frequency of neutral mode is 3.16, and the most unstable frequency is $\omega = 10.8$ with the growth rate of 0.410. In this paper, the frequencies of interest are in the range of $4.0 \le \omega \le 10.8$.

Figures 3-(a) and 4-(a) plot the streamwise distribution of the displacement function for suction velocities $V_{s0} = -0.1$ and -1.0, respectively. The displacement function amplifies in general exponentially, but with a shift on amplitude in the vicinity of X = 0 due to the scattering effect. This phenomenon is not quite obvious for the case of $V_{s0} = -0.1$, but is apparent when the suction velocity increases to $V_{s0} = -1.0$. In order to monitor the scattering effect on the amplitude, we normalize the displacement function by the value in the smooth case $e^{i\alpha X}$, i.e.

$$\mathscr{A}(X) = \tilde{A}(X)e^{-i\alpha X}. \qquad (17)$$

The asymptotic behavior of $\mathscr{A}$ is

$$\mathscr{A}(X) \to \begin{cases} 1 + \overline{P}_0 e^{-i\alpha X} \approx 1 & \text{as } X \to -\infty \\ T & \text{as } X \to \infty \end{cases} \qquad (18)$$

This trend is shown in Fig. 3-(b) and Fig. 4-(b), where we observe the effect of suction on the amplitude near the slot. The 'normalized' displacement function drops to nearly zero for the case of $V_{s0} = -1.0$, indicating a remarkable suppressing effect on the oncoming T-S wave.

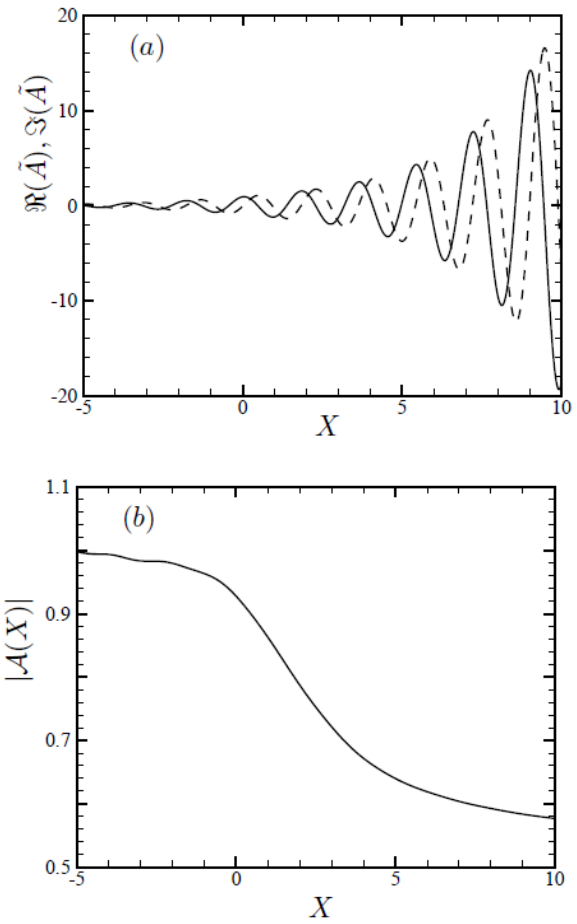

Figure 3 The real (solid line) and imaginary (dashed line) parts of the displacement function (a) and the normalized displacement function (b), where $(V_{s0}, \omega, M, R, d) = (-0.1, 8, 0.2, 10^6, 1)$.

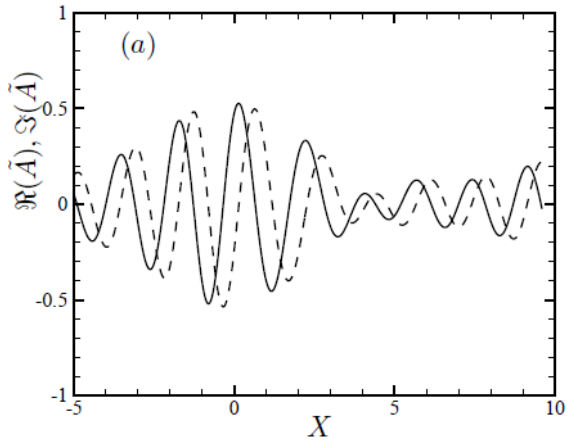

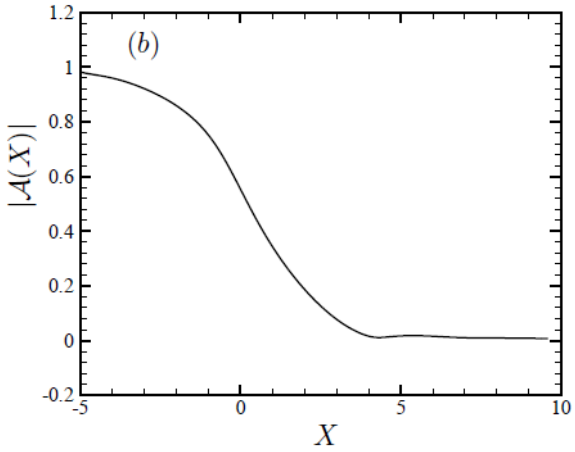

Figure 4 The real (solid line) and imaginary (dashed line) parts of the displacement function (a) and the normalized displacement function (b), where $(V_{s0}, \omega, M, R, d) = (-1.0, 8, 0.2, 10^6, 1)$.

As expected on physical ground, the parameter controlling the contribution to the effect of the T-S wave is the mass flux through the suction/injection slot, which is defined as

$$\mathcal{M} = \int_{-\infty}^{\infty} V_s(X)dX \,. \tag{19}$$

For a Gaussian suction/injection velocity,

$$\mathcal{M} = \sqrt{\pi} dV_{s0} \,.$$

It is found from the calculation that the displacement function and the transmission coefficient only depends on the mass flux of the suction/injection, rather than on the individual suction/injection velocity or slot width.

Fig. 5 shows the transmission coefficient as a function of the mass flux for different frequencies. Only a slightly difference can be observed between the three curves (for different frequencies of interest), implying that the transmission coefficient depends less on the frequency. However, it is strongly dependent of the mass flux. For linear cases, in which the mass flux $\mathcal{M}$ is sufficiently small, the transmission coefficients are 1.0. As $\mathcal{M}$ increases, the transmission coefficient decreases/increases monotonically for suction/ injection cases. When the mass flux becomes O(1), the transmission coefficient is as small as O(0.1) for suction, or as large as O(10) for injection.

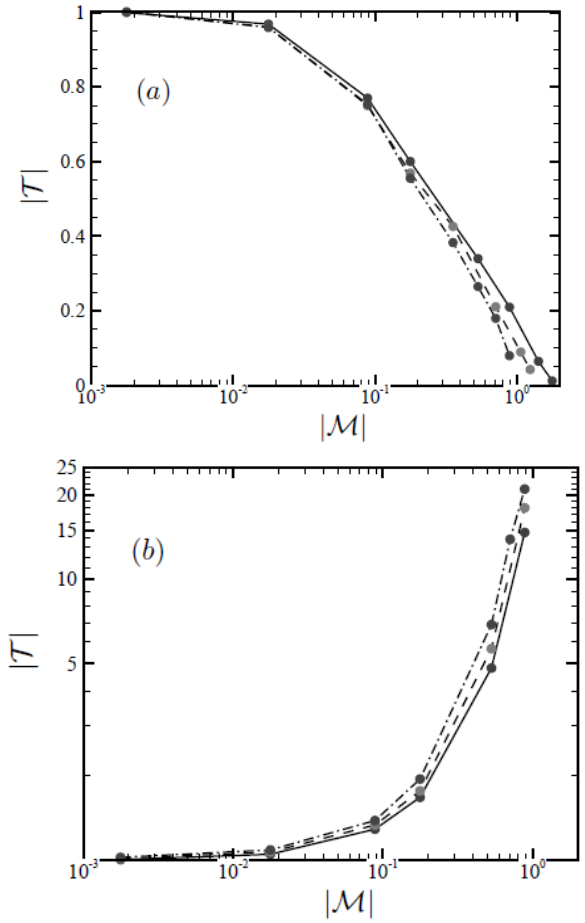

Figure 5 The transmission coefficient vs. suction- (a) and injection- (b) mass flux for $(M, R) = (0.2, 10^6)$. Solid, dashed and dot-dashed lines are for $\omega = 4.0$, 8.0 and 10.8, respectively.

3.3 Acoustic radiation due to the scattering effect

3.3.1 The pressure of the acoustic field

In order for the results to be more accessible to a general reader, the familiar non-dimensional frequency, $f = \omega^* \upsilon_\infty / U_\infty^2 \times 10^6$, will be used in presentation, where ω^* is the dimensional frequency. The global non-dimensional frequency f is related to the local non-dimensional frequency ω by

$$f = \omega \lambda^{3/2} (1 - M^2)^{1/4} C^{-1/4} T_w^{-1} R^{-3/4} \times 10^6 \,.$$

Fig. 6 shows the pressure field of the radiated sound wave for different frequencies. The wavelengths of the radiated acoustic waves are related to the frequencies of the T-S waves. The acoustic directivity for different frequencies seems to be similar, i.e. the radiated sound is

found to be propagating upstream, and an angle of silence about 80 degree is observed. It can also be seen the intensity of the acoustic wave increases with the frequency. A quantitative analysis will be shown in the following sections.

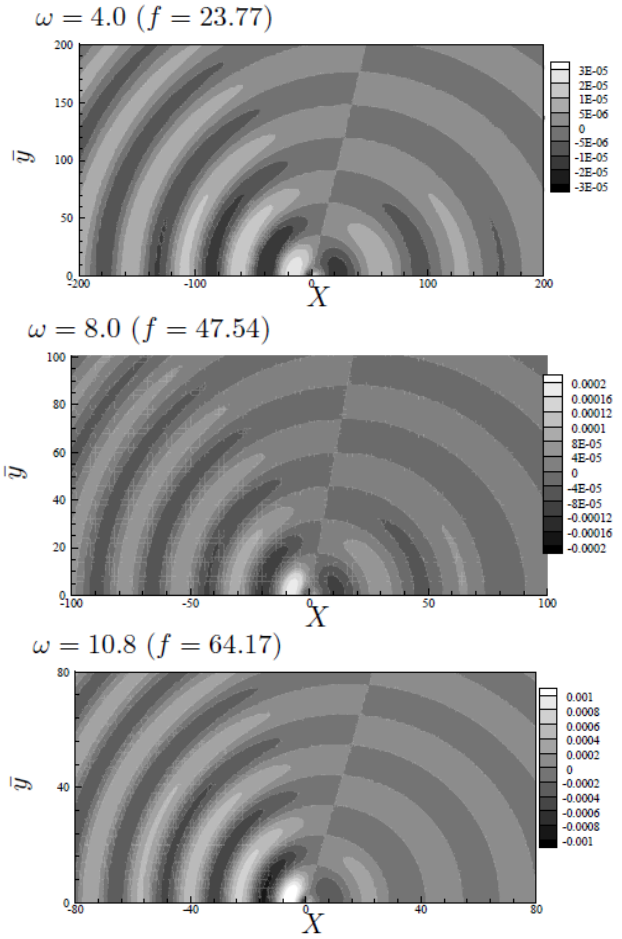

Figure 6 The real part of the pressure of the acoustic field, for $(V_{s0}, M, R, d) = (-0.001, 0.2, 10^6, 1)$

3.3.2 Dependence of acoustic radiation on mass flux

Based on the far-field acoustic pressure (14), the intensity of the sound wave can be measured by

$$Q = p_s \sqrt{\bar{r}}\,. \qquad (20)$$

It is also found that the directivity of the radiated sound wave merely depends on the mass flux of the suction/injection, rather than on the velocity or the slot width.

The directivity of the acoustic field can be better characterized by

$$\tilde{Q} = |Q| / Q_m\,, \qquad (21)$$

where $Q_m = |Q_{\theta=\pi}|$ denotes the upstream propagating sound wave. The normalized directivity of the acoustic field for different suction mass flux are plotted in Fig. 7. In each figure, the difference of the four curves, representing different mass flux, is quite small, i.e. the dominant sound is upstream propagating, and there exists an angle of silence at about 80 degree in each case, indicating that the suction mass flux does not affect substantially the directivity of the emitted sound. However, Q_m varies considerably with the mass flux, as is shown Q_m in Fig. 8. It is found that the acoustic strength in general increases with the mass flux, except for some extreme cases when the suction mass flux is $O(1)$, and the frequency is also high.

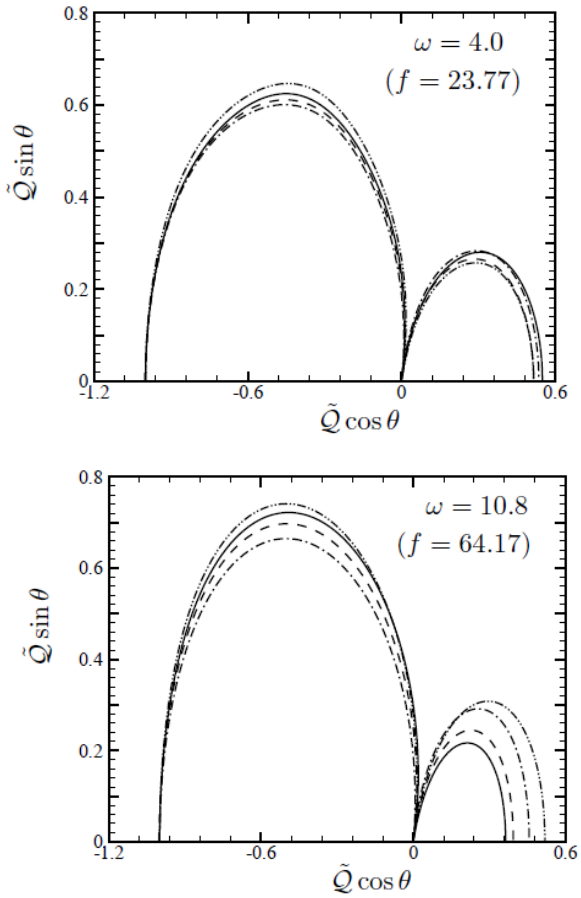

Figure 7 The normalized directivity of the acoustic field as shown by plotting $\tilde{Q}$ in the polar coordinate, where solid, dashed, dot-dashed and dot-dot-dashed lines represent $\mathcal{M} = -0.001\sqrt{\pi}$, $-0.01\sqrt{\pi}$, $-0.1\sqrt{\pi}$ and $-0.5\sqrt{\pi}$.

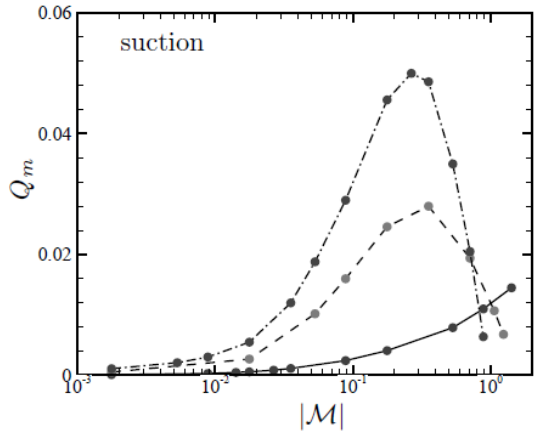

Figure 8 The strength of the upstream radiated sound vs. the suction mass flux. The solid, dashed and dot-dashed lines represent $\omega = 4.0$, 8.0 and 10.8, respectively.

3.3.3 Dependence of acoustic radiation on frequency

Fig. 9 shows the normalized directivity for $\mathcal{M} = -0.01\sqrt{\pi}$ with different frequencies. The directivity behaves similarly for different frequencies, indicating a weak dependence of the former on the latter.

However, the strength of the radiated sound depends strongly on the frequency as is shown in Fig. 10. For a moderate suction mass flux, the acoustic intensity increases with the frequency monotonically. This effect is more pronounced when the mass flux is larger.

3.3.4 Dependence of acoustic radiation on the distribution of the suction velocity

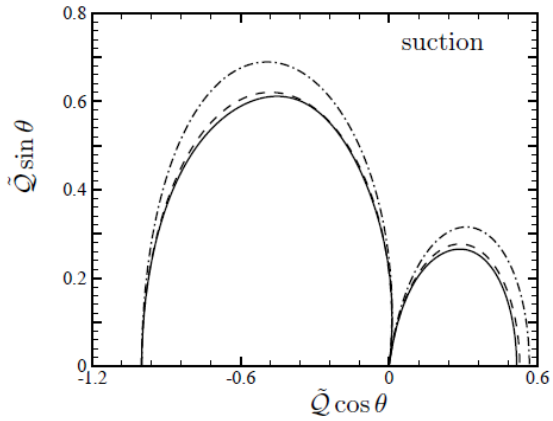

Figure 9 Directivity of the acoustic field as shown by plotting $\tilde{Q}$ in the polar coordinate for $\mathcal{M} = -0.01\sqrt{\pi}$. The solid, dashed and dot-dashed lines represent $\omega = 4.0$, 8.0 and 10.8, respectively.

It is also observed that, if the mass flux is fixed, changing the distribution of the suction velocity does not affect either the scattering effect or the acoustic radiation.

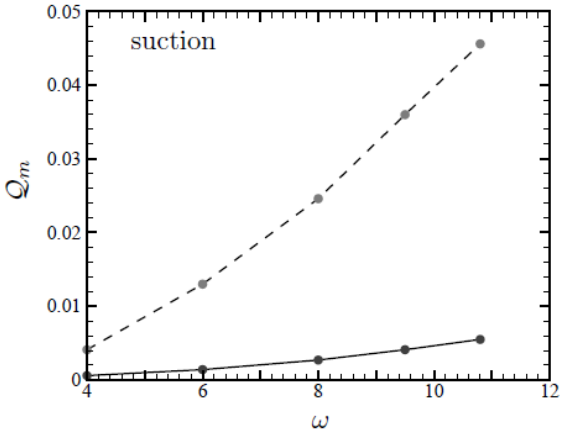

Figure 10 The strength of the upstream radiated sound vs. the frequency for $\mathcal{M} = -0.01\sqrt{\pi}$ (solid line) and $-0.1\sqrt{\pi}$ (dashed line).

4 Concluding remarks

The framework of the Extended Local Scattering Theory is proposed by retaining the unsteady (second-order) terms in the upper-deck governing equations of the triple-deck formalism. The resulting framework describes not only the impact of a local scatter on the hydrodynamic instability but also the acoustic radiation due to scattering of an oncoming T-S wave.

Numerical investigations on the impact of a local steady suction show that suction /injection suppresses/enhances the oncoming T-S waves, with the transmission coefficient decreasing/increasing with the mass flux. The transmission coefficient is of O(0.1) and O(10) when the suction/injection mass flux is of order-one, respectively, implying that transition can be affected significantly by suction or injection on the wall surface. The transmission coefficient is not affected appreciably by the frequency of the oncoming T-S waves.

The Q_m-normalized directivity of the radiated sound wave remains the same, or at least similar, for all the frequencies, mass flux and suction velocity distributions. The dominant acoustic field is on the upstream side, and there exists an angle of silence of about 80 degree.

The intensity of the radiated sound wave depends on both the frequency and the suction mass flux. It is found that, the intensity of the radiated sound increases with the mass flux and frequency, except when $\mathscr{M} = -O(1)$ and the frequency is high. The intensity of the sound wave radiated by the suction slot attains its maximum value at $\mathscr{M} = -O(0.1)$, and becomes weaker when $\mathscr{M} = -O(1)$.

5 References

[1] Wu X and Hogg L**.** Acoustic radiation of Tollmien-Schlichting waves as they undergo rapid distortion. *J Fluid Mech,* Vol. 550, pp 307-347, 2006.

[2] Stewartson K. Multi-structured boundary layers on flat plates and related bodies. *Adv Appl Mech,* Vol. 14, pp 145-239, 1974.

[3] Smith F. On the non-parallel flow stability of the Blasius boundary layer. *Proc R Soc Lond,* Vol. 366, pp 91-109, 1979.

[4] Wu X and Dong M. A local scattering theory for the effect of isolated roughness on boundary layer instability and transition: transmission coefficient as an eigen-value. *J Fluid Mech*, Vol. 794, pp 68-108, 2016.

[5] Wu X. On generation of sound in wall-bounded shear flows: back action of sound and global acoustic coupling. *J Fluid Mech*, Vol. 689, pp 279-316, 2011.

[6] Dong M and Wu X. Acoustic radiation due to scattering of a T-S wave by nonlinear roughness in a subsonic boundary layers. *AIAA P*. AIAA-2015-2626, 2015.

6 Acknowledgements

This research is supported by Marie Curie Fellowship (H2020-MSCA-IF-2014, grant 659328).

7 Copyright Statement

8 Contact Author Email Address

mailto:x.wu@ic.ac.uk